Stability of a Jet in Confined Pressure-Driven Biphasic Flows at Low Reynolds Numbers

Pierre Guillot,[1,*] Annie Colin,[1] Andrew S. Utada,[2] and Armand Ajdari[3,†]

[1]*Rhodia Laboratoire du Futur, Unité mixte Rhodia-CNRS, Université Bordeaux I, 178 Avenue du Docteur Schweitzer, 33608 Pessac, France*

[2]*School of Engineering and Applied Sciences, Harvard University, Cambridge, Massachusetts 02138, USA*

[3]*Gulliver, UMR CNRS-ESPCI 7083, 10 rue Vauquelin, 75231 Paris Cedex 05, France*

(Received 1 November 2006; published 7 September 2007)

Motivated by its importance for microfluidic applications, we study the stability of jets formed by pressure-driven concentric biphasic flows in cylindrical capillaries. The specificity of this variant of the classical Rayleigh-Plateau instability is the role of the geometry which imposes confinement and Poiseuille flow profiles. We experimentally evidence a transition between situations where the flow takes the form of a jet and regimes where drops are produced. We describe this as the transition from convective to absolute instability, within a simple linear analysis using lubrication theory for flows at low Reynolds number, and reach remarkable agreement with the data.

DOI: 10.1103/PhysRevLett.99.104502 PACS numbers: 47.15.Fe, 47.55.−t, 47.61.Jd, 83.50.Ha

Since the seminal works of Plateau [1] and Rayleigh [2], i.e., for more than a century, the breakup of a liquid jet injected in an immiscible liquid has been extensively investigated because of its relevance for an immense field of practical and industrial applications ranging from chemical processes to ink jet printing, through spray atomization, emulsification process, and polymer extrusion, to name a few. A major result is that inviscid cylindrical jets in air are unstable to disturbances of wavelength larger than the jet circumference. The interplay of interfacial stresses and inertial forces that rules jet breakup is rather complex [3,4], and can be rationalized in terms of absolute and convective instabilities as determined from a linear analysis [5]. An absolute instability corresponds to disturbances growing and propagating both downstream and upstream, leading after a transient to drops released at or close to the injection nozzle. Increasing velocity sufficiently can make the instability convective with perturbations that propagate downstream while they grow, allowing for a continuous fluid thread to persist. Several experimental studies support this picture [6,7].

In this Letter, we apply these concepts to analyze jet stability in a somewhat different realm, namely, biphasic flows in microfluidic channels. In this context, dripping and coflow regimes have been not only observed, but also exhaustively used for various applications [8–10]. Beyond the importance of viscous forces (the Reynolds numbers are typically small to moderate), the essential contrast with most of the previous studies which focused on unbounded flows [6,11–13] is the major role of the microchannel walls which induce parabolic flow profiles and strongly affect the development of perturbations.

In our experiments, we generate a jet in a cylindrical glass capillary of inner radius R_c, using as a nozzle a glass capillary of square cross-section with a tapered end (see Fig. 1). The outer dimension of this square capillary is very close to the inner diameter of the cylindrical tube which ensures good alignment and centering [14]. R_c is in the 200–500 μm range, whereas the radius of the tapered orifice of the square tube is set between 20 and 50 μm using a pipette-puller set up. Syringe pumps are used to inject an inner fluid of viscosity η_i at a rate Q_i in the square capillary and the outer fluid of viscosity η_e at a rate Q_e through the cylindrical capillary. This leads to coaxial injection at the tapered orifice.

We observe flow patterns which vary significantly with operational (Q_e, Q_i), geometrical (R_c), and system parameters (η_i, η_e, surface tension Γ). Figure 2 displays the typical outcome of an experiment where the flow rates are varied for a given system (here the inner solution is a 50% in weight glycerine in water solution with $\eta_i =$ 55 mPa.s and the outer one a silicone oil for which $\eta_e =$ 235 mPa.s). A droplet regime is found for low Q_i, with either droplets emitted periodically right at the nozzle—symbol (open circle)—or non spherical pluglike droplets resulting from the instability of an emerging oscillating jet (filled gray circle). Jets are found in the bottom right corner of Fig. 2 with different visual aspects: wavy jets with features that are convected downstream (open square), and for larger values of Q_i, straight jets (filled square) that persist throughout the cylindrical capillary. For large values of the external flow rate Q_e, we observe what we call jetting: thin and rather straight jets (open diamond) that extend over some distance in the capillary tube before

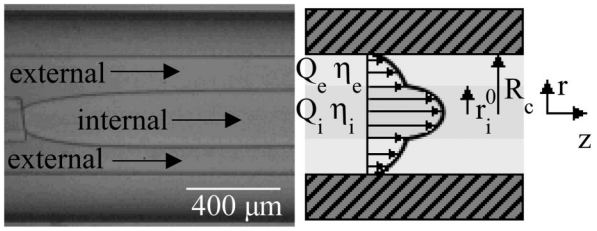

FIG. 1. Flow geometry and notations used in the text.

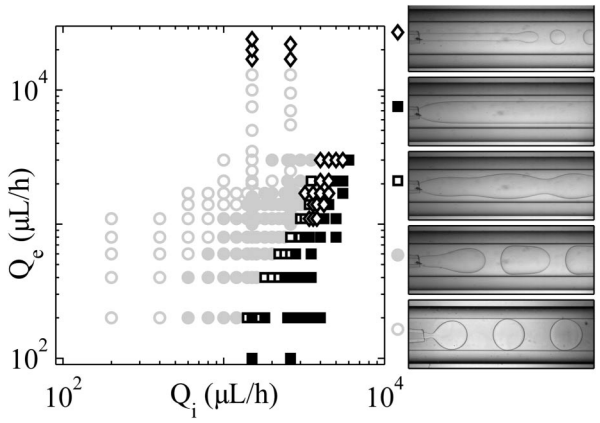

FIG. 2. Map of the flow behavior in the (Q_i, Q_e) plane. The droplet regime comprises droplets smaller than the capillary (open circle) and pluglike droplets confined by this capillary (filled circle). Jets are observed in various forms: jets with visible peristaltic modulations convected downstream (open square), wide straight jets (filled square) that are stable throughout the ~5 cm long channel, and thin jets breaking into droplets at a well-defined location (open diamond). Parameters are $R_c = 275\ \mu$m, inner viscosity $\eta_i = 55$ mPa.s, outer viscosity $\eta_e = 235$ mPa.s, surface tension $\Gamma = 24$ mN/m.

breaking into droplets at a well-defined and reproducible location. This "jet length" increases with Q_i for a fixed value of Q_e [15]. Similar "dynamic phase diagrams" have been reported for more complex microfluidic geometries [16–20].

We now attempt to model these phenomena analytically, taking advantage of the simplicity and symmetry of the present cylindrical geometry. The problem remains however quite complex, even at the level of a linear stability analysis, so we proceed with approximations [21]. We neglect inertial effects (i.e., as the Reynolds number is small in most of our experiments), and we use lubrication theory (i.e., we formally assume that the wavelengths of the perturbations are long compared to the capillary radius) which has been shown to be remarkably insightful in somewhat related situations [22]. The unperturbed reference state (Fig. 1) is easily described using Stokes equation. The pressure gradients in the two fluids are for this unidirectional flow constant and equal $\partial_z P_e = \partial_z P_i = \partial_z P^0$, with the Laplace law relating the local pressures: $P_i^0 - P_e^0 = \frac{\Gamma}{r_i^0}$ where r_i^0 the radius of the inner jet (Fig. 1). We perform a linear stability analysis of this solution, considering only small z-dependent cylindrically symmetric perturbations $\delta r_i(z, t)$. Within the lubrication approximation (i.e., assuming that the interface is flat and that the flow is uunidirectional), this leads to a description in terms of the resulting perturbations $\delta Q_e(z, t)$, $\delta Q_i(z, t)$, $\partial_z \delta P_e(z, t)$, $\partial_z \delta P_i(z, t)$, which are locally related by relations similar to those describing the unperturbed flow. In particular, we still enforce no slip boundary condition at the solid liquid interface as well as continuity of the velocity and of tangential stress at the interface between the two fluids. The important difference is that, as the radius of the jet varies, so does, through the Laplace law, the difference between the two pressure gradients:

$$\partial_z(\delta P_i - \delta P_e) = -\Gamma\, \partial_z\left(\frac{\delta r_i}{r_i^{02}} + \partial_z^2 \delta r_i\right) \tag{1}$$

with $\partial_z^2 \delta r_i$ and $\frac{\delta r_i}{r_i^{02}}$ the jet curvatures along and perpendicular to the flow. Mass conservation of the incompressible fluids provides the closure of the system of equations: $\delta Q_e(z, t) + \delta Q_i(z, t) = 0$ and $\partial_t \pi (r_i^0 + \delta r_i)^2 = -\partial_z((\delta Q_e(z, t))$.

Considering perturbations proportional to $e^{(ikz+\omega t)}$, with $k = k_r + ik_i$ and $\omega = \omega_r + i\omega_i$ complex numbers, we obtain the dispersion equation:

$$\tilde{\omega} = \frac{-i\,Ka\; x^3 E(x, \lambda)\tilde{k} + F(x, \lambda)(\tilde{k}^2 - \tilde{k}^4)}{x^9(1 - \lambda^{-1}) - x^5} \tag{2}$$

where we use the notations $\tilde{k} = r_i^0 k$, $\tilde{\omega} = \frac{\omega 16 \eta_e R_c}{\Gamma}$,

$$E(x, \lambda) = -4x + (8 - 4\lambda^{-1})x^3 + 4(\lambda^{-1} - 1)x^5,$$

$$F(x, \lambda) = x^4[4 - \lambda^{-1} + 4\ln(x)] + x^6(-8 + 4\lambda^{-1}) + x^8[4 - 3\lambda^{-1} - (4 - 4\lambda^{-1})\ln(x)],$$

and where we identify the three essential adimensional parameters that rule the behavior of the system: the viscosity ratio $\lambda = \frac{\eta_i}{\eta_e}$, the degree of confinement of the unperturbed jet $x = \frac{r_i^0}{R_c} = \sqrt{\frac{\alpha - 1}{\lambda^{-1} + \alpha - 1}}$ with $\alpha = \sqrt{1 + \lambda^{-1}\frac{Q_i}{Q_e}}$, and a capillary number $Ka = \frac{-\partial_z P^0 R_c^2}{\Gamma}$. Note that Ka is a capillary number defined at the scale R_c and not at the jet scale r_i^0 as in most studies of unbounded flows.

The jet would be linearly stable if all ω_r were negative, which is not the case. With some ω_r positive, an initially localized perturbation generates a growing distortion that spreads in a domain bounded by two fronts moving at velocities v_+^* and v_-^*, selected because they correspond to maximal growth rate ω_r and extremal velocity of the envelope of the perturbation $v = \frac{\omega_r}{k_i}$. These criteria read $v^* = \frac{\omega_r^*}{k_i^*}$, $\frac{\partial \omega_r^*}{\partial k_r} = 0$ and $v^* = \frac{\partial \omega_r^*}{\partial k_i}$ [5,22], which selects, in a dimensional form $\tilde{v}^* = \tilde{\omega}_r^*/\tilde{k}_i^*$,

$$\tilde{v}_{\mp}^* = \frac{Ka\, x^3 E(x, \lambda) \mp C_1 F(x, \lambda)}{x^9(1 - \lambda^{-1}) - x^5} \tag{3}$$

where $C_1 = \frac{5+\sqrt{7}}{18}\sqrt{\frac{24}{\sqrt{7}-1}}$.

As v_+^* is always positive, the nature of the instability is set by the sign of v_-^*: if negative, growing perturbations also travel backwards and the jet is absolutely unstable, while for $v_-^* > 0$, the instability is convective as all perturbations are convected downstream. We reach a rather simple analytical prediction for the transition: $\tilde{v}_-^*(Ka, x, \lambda) = 0$, plotted on Fig. 3 in the (x, Ka) plane describing operational conditions, for various values of the system dependent viscosity ratio $\lambda = \eta_i/\eta_e$.

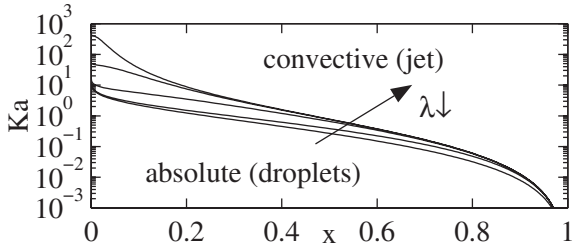

FIG. 3. Dynamic behavior diagram in the (x, Ka) plane. The lines are the predictions $\tilde{v}_-^*(Ka, x, \lambda) = 0$ for the absolute-convective transition, for viscosity ratios λ equal to 10, 1, 0.1, 0.01, and 0.001 (bottom to top). Above the lines, the jet is convectively unstable, whereas below the lines, the jet is absolutely unstable. Regions below the lines correspond to droplets region.

We suggest that this plot describes the dynamic behavior of our system, with the transition separating dripping (absolute instability) from jets (convective instability). Indeed, in the convective case, growing disturbances are simultaneously convected downstream and a continuous jet can persist in the system over some distance (which does not preclude the formation of droplets downstream). This encompasses the three types of jets observed in Fig. 2. By contrast, in the absolute instability regime, no jet is stable, as any perturbation generates oscillations that grow and travel backwards to invade the whole capillary. This corresponds to the droplets and plugs regimes displayed on Fig. 2.

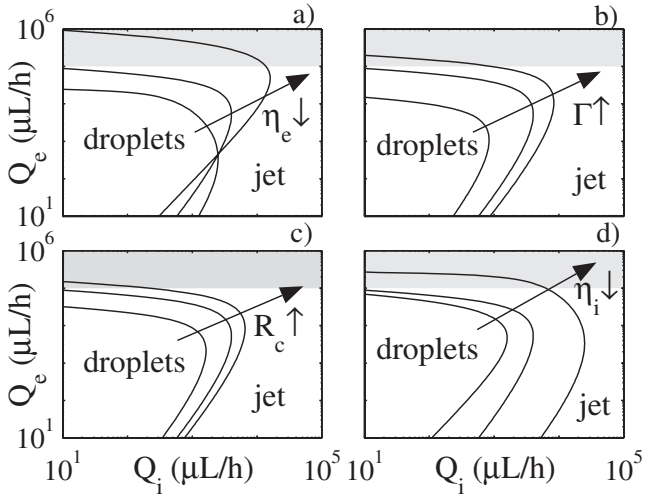

FIG. 4. Dynamic behavior in the (Q_i, Q_e) plane from our simple model. Above the line, the jet is convectively unstable, whereas below the lines it is absolutely unstable and droplets are expected. We vary independently each parameter around the conditions of Fig. 2 chosen as reference: $\Gamma = 24$ mN/m, $R_c = 275$ μm, $\eta_e = 235$ mPa.s and $\eta_i = 55$ mPa.s. (a) From top to bottom, $\eta_e = 23.5$, 235 and 2350 mPa.s. (b) From top to bottom, $\Gamma = 50$, 24 and 5 mN/m. (c) From top to bottom, $R_c = 350$, 275 and 175 μm. (d) From top to bottom, $\eta_i = 5.5$, 55 and 550 mPa.s. The gray shading indicates where the average Reynolds number is larger than unity [24].

What are the main features predicted by this model? Comparing systems, decreasing $\lambda = \eta_i/\eta_e$ increases the "droplet" regime at the expense of the "jet" regime. For a given system (a given λ), one moves from droplets to jets, either by increasing the capillary number Ka (i.e., the normalized pressure drop) or the degree of confinement $x = r_i^0/R_c$. This is physically sound, as increasing Ka corresponds to convecting away the perturbations faster, while increasing the confinement x results in slowing down the rate of development of the perturbations due to the proximity of the walls.

In order to provide a directly useful guide, we turn to a representation in the operational plane Q_i, Q_e, in the Fig. 4 using characteristic values of our experiments. Noticeably, these plots predict a "reentrant" behavior jet → drops → jet upon increase of the external flow rate Q_e with all other parameters fixed. This relies on the physics mentioned above. At low Q_e, increasing Q_e mostly reduces the strong confinement of the jet, allowing the instability to develop faster and thus promoting the formation of droplets. At high Q_e, confinement is not significant, and raising Q_e primarily increases the jet velocity and the downstream

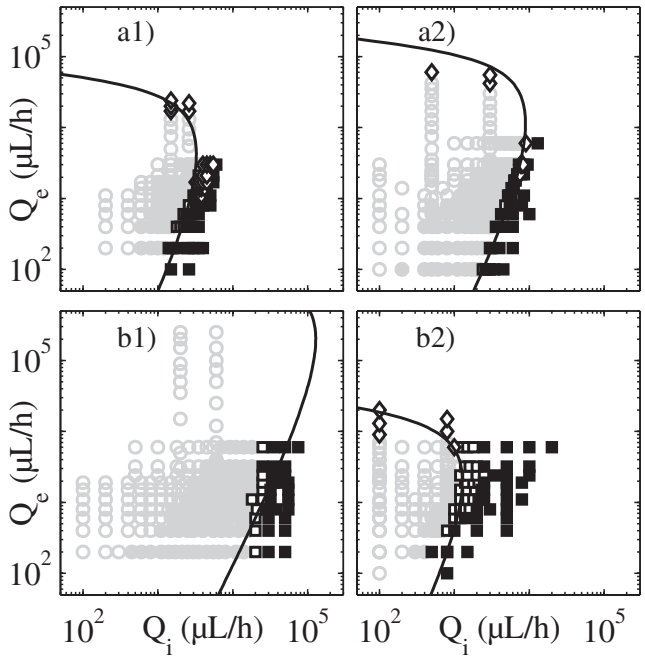

FIG. 5. Experimental data (symbols) and theoretical predictions (continuous line) displaying the effect on the dynamical behavior of an increase of the capillary radius R_c [(a1) → (a2)] and a decrease of the surface tension Γ [(b1) → (b2)]. Gray symbols (open gray circle and filled gray circle) correspond to droplets and the black ones (open square, filled square, and open diamond) to jets (see Fig. 2). For (a1) and (a2), $\Gamma = 24$ mN/m, $\eta_e = 0.235$ Pa.s and $\eta_i = 0.055$ Pa.s, with $R_c = 275$ μm for (a1) and $R_c = 435$ μm for (a2). For (b1) and (b2), $R_c = 275$ μm, $\eta_e = 3$ mPa.s and $\eta_i = 1$ mPa.s, with $\Gamma = 12$ mN/m in (b1), and a decreased value using surfactants $\Gamma = 0.12$ mN/m in (b2). The lines are obtained without adjustable parameters.

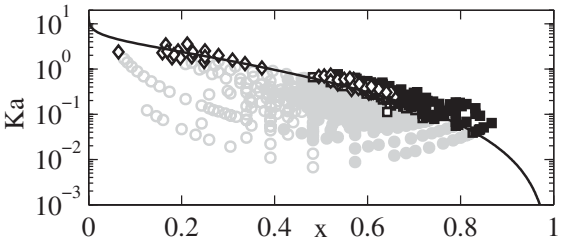

FIG. 6. Flow behavior in the (x, Ka) plane for a given value of the viscosity ratio $\lambda = 0.23$. x is calculated from the first order solution using the experimental values of the flow rates and viscosities. The data (symbols as in Figs. 2 and 5) correspond to two radii and two surface tensions. The line is the theoretical prediction of our linear analysis for the droplets/jet transition, with no adjustable parameters.

convection of any developing perturbation, which favors a continuous jet. These plots also clarify the influence of the various parameters. For given flow rates, droplet formation is promoted by large surface tension, wide capillaries, and large internal viscosity, while the influence of the external viscosity depends on the flow rates considered [see Fig. 4(a)].

We now *quantitatively* compare our predictions to experimental data obtained for three surface tensions, two viscosity ratios, and two capillary radii R_c (Fig. 5). Clearly, given the approximations involved, our simple model describes very well the experimental data *with no adjustable parameters*, and appears as a powerful predictive tool. A certain level of disagreement is expected for weak confinement (small Q_i large Q_e) as the lubrication approximation is formally invalid in this case. Our model indeed overestimates Ka at the transition for vanishing x, as demonstrated by comparison to the exact result of Gañán-Calvo [23] for unbounded creeping flows. Inertial effects may also slightly alter the picture for the largest outer flow rates (see the shaded areas in Fig. 4). We also report in Fig. 6 all the experimental data obtained for a given viscosity ratio λ, but for various surface tensions, various capillary radii, and various flow rates. This shows the relevance of our description in terms of the adimensional variables Ka and x. An additional interest of this mapping onto the (Ka, x) plane of this large set of data is that it collapses relatively well the different types of flows observed within the droplets and jets regimes as can be seen by the grouping of the symbols. In short, droplets correspond to small capillary number Ka and small confinement ratio x, while plugs require larger values of x. At higher values of Ka, increasing the confinement ratio x shifts the behavior from "jetting" (with emission of droplets at a large finite distance from the nozzle) to stable jets.

In conclusion, we have studied a variant of the Rayleigh Plateau problem, i.e., the stability of pressure-driven concentric jets in a cylindrical confining geometry at low Reynolds numbers. We have demonstrated that the nature of the instability at the linear level (absolute or convective) controls whether drops or a jet are obtained in this situation. We have identified the relevant adimensional quantities that control the dynamic behavior and obtained analytical predictions for the locus of the transition as a function of all the involved physical and operational parameters. Both agree quantitatively with our experiments, yielding a predictive synthetic map of the dynamic behavior and of the resulting flow patterns. Returning to microfluidic applications, we expect this mapping to be robust and relevant for more commonly used microchannels, which have cross-sections of lower symmetry (square, rectangular, ...). The corresponding experimental and theoretical investigation is under way.

The authors gratefully acknowledge support from the Région Aquitaine, and warmly thank D. A. Weitz for his interest and hospitality and M. Joanicot for his constant support.

*pierre.guillot@eu.rhodia.com
†Corresponding author: armand.ajdari@espci.fr

[1] J. Plateau, *Statique Experimentale et Theorique des Liquides soumis aux Seules Forces Moleculaires* (Gauthier-Villars, Paris, 1873), pp. 450–495.
[2] Lord Rayleigh, Proc. London Math. Soc. **s1-10**, 4 (1878).
[3] S. P. Lin *et al.*, Annu. Rev. Fluid Mech. **30**, 85 (1998).
[4] J. Eggers, Rev. Mod. Phys. **69**, 865 (1997).
[5] W. van Saarloos, Phys. Rev. A **37**, 211 (1988); **39**, 6367 (1989).
[6] J. M. Gordillo *et al.*, J. Fluid Mech. **448**, 23 (2001).
[7] I. Vihinen *et al.*, Phys. Fluids **9**, 3117 (1997).
[8] B. Zheng *et al.*, J. Am. Chem. Soc. **125**, 11170 (2003).
[9] M. Joanicot and A. Ajdari, Science **309**, 887 (2005).
[10] P. Guillot *et al.*, Langmuir **22**, 6438 (2006).
[11] A. Sevilla *et al.*, Phys. Fluids **17**, 018105 (2005).
[12] A. M. Gañán-Calvo *et al.*, Phys. Rev. Lett. **96**, 124504 (2006).
[13] A. M. Gañán-Calvo *et al.*, J. Fluid Mech. **553**, 75 (2006).
[14] A. S. Utada *et al.*, Science **308**, 537 (2005).
[15] We consider that we have a jet whenever there is a continuous jet section, wavy or not, the length of which is longer than 3 times the eventual droplet size (if any).
[16] T. Thorsen *et al.*, Phys. Rev. Lett. **86**, 4163 (2001).
[17] C. Cramer *et al.*, Chem. Eng. Sci. **59**, 3045 (2004).
[18] J. D. Tice *et al.*, Anal. Chim. Acta **507**, 73 (2004).
[19] S. L. Anna *et al.*, Appl. Phys. Lett. **82**, 364 (2003).
[20] P. Guillot and A. Colin, Phys. Rev. E **72**, 066301 (2005).
[21] This is equivalent to a computation of the linear response in δr_i through a second order expansion in powers of kR_c of the velocity field, where k is the axial wavelength of the perturbation, with an additional approximation. Specifically, in the calculation of the $O[(kR_c)^2]$ term, we neglect the pressure gradient created by the zero order in kR_c velocity compared to that generated by the interface curvature along z. This is valid for the data discussed here (discussion postponed for a forthcoming paper).
[22] T. R. Powers *et al.*, Phys. Rev. Lett. **78**, 2555 (1997).
[23] A. M. Gañán-Calvo, Phys. Rev. E **75**, 027301 (2007).
[24] We use the simple estimate $\mathrm{Re} = [\rho(Q_e^2/\eta_e + Q_i^2/\eta_i)]/[\pi R_c(Q_e + Q_i)]$ and $\rho = 1000\ \mathrm{kg/m^3}$.